Journal of controlled release

Novel cyclic peptides facilitating transcellular blood-brain barrier transport of macromolecules *in vitro* and *in vivo*

Shunsuke Yamaguchi[1,2], Shingo Ito[1,3], Takeshi Masuda[1,3], Pierre-Olivier Couraud[4], Sumio Ohtsuki[1,3]*

[1]Department of Pharmaceutical Microbiology, Graduate School of Pharmaceutical Sciences, Kumamoto University, 5-1 Oe-honmachi, Chuo-ku, Kumamoto 862-0973, Japan
[2]Japan Society for the Promotion of Science, Research Fellowship for Young Scientists, Chiyoda-ku, Tokyo, Japan
[3]Department of Pharmaceutical Microbiology, Faculty of Life Sciences, Kumamoto University, 5-1 Oe-honmachi, Chuo-ku, Kumamoto 862-0973, Japan
[4]Institut Cochin, INSERM U1016, CNRS UMR8104, Université Paris Descartes, Sorbonne Paris Cité, Paris, France

*Corresponding author: Sumio Ohtsuki, Ph.D
Department of Pharmaceutical Microbiology, Faculty of Life Sciences, Kumamoto University, 5-1 Oe-honmachi, Chuo-ku, Kumamoto 862-0973, Japan
TEL: +81-96-371-4323; FAX: +81-96-371-4329; E-mail: sohtsuki@kumamoto-u.ac.jp

1. Abstract

Brain delivery of nanoparticles and macromolecular drugs depends on blood-brain barrier (BBB)-permeable carriers. In this study, we searched for cyclic heptapeptides facilitating BBB permeation of M13 phages by phage library screening using a transcellular permeability assay with hCMEC/D3 cell monolayers, a human BBB model. The M13 phage, which is larger than macromolecular drugs and nanoparticles, served as a model macromolecule. The screen identified cyclic heptapeptide SLSHSPQ (SLS) as a human BBB-permeable peptide. The SLS-displaying phage (SLS-phage) exhibited improved permeation across the cell monolayer of monkey and rat BBB co-culture models. The SLS-phage internalized into hCMEC/D3 cells via macropinocytosis and externalized via the exosome excretion pathway. SLS-phage distribution into brain parenchyma was observed in mice after intravenous administration. Moreover, liposome permeated across the BBB as cyclic-SLS-peptide conjugates. In conclusion, the cyclic SLS heptapeptide is a novel carrier candidate for brain delivery of macromolecular drugs and nanoparticles.

Keywords: Cyclic peptide, Phage display technology, Brain delivery, Macromolecule

2. Introduction

Macromolecular drugs, such as antibodies or nucleic acids, are considered candidates for molecularly targeted drugs that are actively studied in basic and clinical research [1-3]. However, their low permeability across the blood-brain barrier (BBB) hinders the clinical application for central nervous system (CNS) diseases. The BBB, consisting of brain capillary endothelial cells linked by tight junctions, prevents the entry of various therapeutics, including proteins and nucleic acids, into the brain. In fact, nearly all of the macromolecular drugs are unable to cross the BBB [4, 5]. Thus, delivery carrier systems that improve BBB permeability are needed for the development of CNS-acting drugs, especially for macromolecular drugs.

To date, several BBB-permeable carriers, such as monoclonal antibodies (MAbs) and peptides, have been reported. Transferrin receptor (TfR) is transcytosed across the BBB via clathrin, and Pardridge *et al*. reported that a MAb against rat and human TfR (OX26) penetrated the brain parenchyma by crossing the BBB [6]. In addition, MAbs against insulin receptor and low-density lipoprotein receptor-related protein 1 (LRP1) can also function as BBB-permeable carriers via clathrin and caveolae, respectively [7-9]. Angiopep-2, a peptide carrier derived from LRP1 ligand aprotinin, permeated the BBB via LRP-1, and angiopep-2-conjugated paclitaxel displayed increased anti-tumor efficacy against glioma compared to that of paclitaxel [10, 11]. However, the size range of clathrin- or caveolae-mediated endosomes of approximately 50–100 nm is smaller than that of nanoparticles, such as liposomes of approximately 100-200 nm [12]. Therefore, the carriers utilizing endocytosis have a size limitation for cargo destined for brain delivery.

Cationic cell-penetrating peptides (CPPs) are the peptide carriers facilitating internalization into the cells by macropinocytosis [13-16]. However, utilizing macropinocytosis for brain delivery of macromolecules is a rational strategy because macropinosomes are approximately 5 μm in size [12, 17, 18]. Indeed, one cationic CPP, the Tat peptide, functioned as a brain delivery carrier of macromolecules using *in vivo* models of ischemia and seizure [19-23]. In contrast, Simon *et al.* found that the Tat peptide could not deliver the green fluorescent protein (GFP) across the intact BBB *in vitro* [24]. These results suggested that the brain entry of Tat peptide was associated with the BBB breakdown during CNS diseases, such as ischemia and seizure. The cationic CPPs cause cytotoxicity [25], and the Tat peptide is known to disrupt BBB integrity [26-33]. Furthermore, cationic CPPs can also escape from macropinosomes to the cytosol by electrostatic interaction with the negatively charged macropinosome membrane where they are trapped in intracellular organelles, which would attenuate the delivery efficiency of CPP-conjugated molecules to the brain [34-36]. Indeed, cationic nanosized beads (500 nm) modified with polymer polyethyleneimine (PEI) are internalized into the BBB but not transcytosed to the brain parenchyma [37]. Hence, a new BBB-permeating carrier system enabling the delivery of macromolecular drugs and nanoparticles to the brain is still needed.

We recently identified the anionic cyclic DNPGNET heptapeptide (DNP) by a phage library screening, which improved the permeability of M13 phage and non-permeable fluorescein FAM across the intestinal epithelium [38]. Our previous study demonstrated that non-cationic peptides, including DNP, could permeate across the cell monolayer of Caco-2 cells and the intestinal epithelium in mice, suggesting the possibility that transcellular permeable peptides differ in their properties, including charge, from CPPs. Furthermore, the M13 phage (approximately 1 μm) is larger than clathrin- and caveolae-mediated endosomes, and macropinocytosis was involved in facilitating the transcellular permeation of phages displaying the identified cyclic peptides [38-40]. Hence, phage library screening using a transcellular permeability assay appears to be a rational tool for identifying new non-cationic BBB-permeable peptide carriers exploiting macropinocytosis. Moreover, cyclic peptides typically have a higher affinity for target molecules and better stability against proteases than linear peptides [41], which are favorable properties for BBB-permeable carrier peptides.

Thus, the objective of this study was to identify novel cyclic heptapeptides for improving the BBB permeability of macromolecules by combining phage display screening with a transcellular permeability assay with hCMEC/D3 cells as the human BBB model. The hCMEC/D3 cells are immortalized human cerebral microvascular endothelial cells that reportedly retain the expression of receptors, transporters, and tight-junction proteins typically found in isolated human brain capillaries [42]. We further investigated the permeability of a newly identified cyclic heptapeptide candidate across the BBB *in vitro* and *in vivo*.

3. Materials and Methods

Reagents

Ph.D.™-C7C Phage Display Peptide Library was obtained from New England Biolabs (Ipswich, UK). In the library, the heptapeptide inserts were cyclized by a disulfide bond between an N- terminal and a C-terminal cysteine residue, and they were linked to the minor coat protein (pIII) with a GGGS spacer in M13 phage. The cyclic peptide AC-SLSHSPQ-CGGGS (cyclic SLS derivative), cyclizing between two cysteines by a disulfide bond, was purchased from GenScript (Tokyo, Japan). Fluorescent cyclic SLS derivative (AC-SLSHSPQ-CGGGS) labeled with 5/6-FAM at the C-terminus (fluorescent SLS peptide) and stearyl cyclic SLS derivative (AC-SLSHSPQ-CGGGS) modified with stearic acid at the C-terminus (SLS-STR peptide) were purchased from Scrum (Tokyo, Japan).

Cell culture

The hCMEC/D3 cells were derived from an immortalized human brain capillary endothelial cell line [43]. They were cultured on collagen type I–coated dishes using endothelial cell growth basal medium-2 (EBM-2, Lonza, Walkersville, MD). EBM-2 was supplemented with 1% penicillin-streptomycin (Wako), 5% fetal bovine serum (FBS; Nichirei Bioscience Inc., Tokyo, Japan), 1.4 μM hydrocortisone (Sigma-Aldrich, St. Louis, MO), 1% chemically defined lipid concentrate (Gibco/Invitrogen, Carlsbad, CA), 5 μg/mL ascorbic acid (FUJIFILM Wako Pure Chemical Corporation, Osaka, Japan), 10 mM lithium chloride (Wako), 10 mM HEPES (Sigma-Aldrich), and 1 ng/mL human basic fibroblast growth factor (Sigma-Aldrich). The incubation was performed in an atmosphere of 95% air and 5% CO_2 at 37 °C. The medium was changed 2–3 times a week after seeding.

In vitro phage library screening

hCMEC/D3 cells (2.0×10^5 cells per well) were cultured on membrane inserts in 6-well Transwell plates (Corning, New York, USA) for 5–7 days by changing the culture medium every 2-3 days. Tight-junction integrity was assessed by transepithelial electrical resistance (TEER) with a Millicell ERS-2 (Merck Millipore, Bedford, MA). The hCMEC/D3 cell monolayer, of which the TEER value was above 100 $\Omega \times cm^2$, was used. After pre-incubation of the cell monolayer with fresh EBM-2 for 10 min at 37 °C, the medium the apical side (luminal side) was replaced to the EBM-2 containing the phage library (1.0×10^{11} pfu). The insert was transferred to fresh well at an indicated time to avoid reverse transport from the basal side (abluminal side). Then, a plaque assay was performed to count the number of phages permeated on the basal side, as described in the instructions by manufacturer. For the next round, the permeated phages were amplified using conventional methods according to the manual. Using amplified phages, the phage library screening with hCMEC/D3 cells was repeated three times. After the 3rd screening, each phage DNA was isolated from a single plaque, and the cDNA fragments of heptapeptides were amplified by means of PCR with primers (5′-CCCTCATAGTTAGCGTAACG-3′ and 5′-TTCGCAATTCCTTTAGTGGT-3′) and PrimeSTAR GXL DNA polymerase (Takara Bio, Shiga, Japan). The amplified cDNA fragments were sequenced and the amino acid sequences of the phage-displayed cyclic heptapeptides were derived from DNA sequencing results.

In vitro BBB permeability assay

hCMEC/D3 cell monolayers were prepared on 6-well Transwell plates and incubated as noted in the preceding subsection. After pre-incubation, each phage clone in EBM-2 was

subjected to the apical side (1.0×10^{11} pfu). The amount of permeated phages on the basal side at discrete timepoints was quantitated by the standard curve method using data obtained from qPCR using the Prime Time® qPCR Assay kit (5′-/56-FAM/CGGCCGAAA/Zen/CTGTTGAAAGTTGTTTAGC/3IABkFQ/-3′ for Prime Time probe; 5′-CCCTCATAGTTAGCGTAACG-3′ and 5′-TTCGCAATTCCTTTAGTGGT-3′ for primers) (IDT, San Jose, USA). hCMEC/D3 cell monolayers were prepared on 12-well Transwell plates in inhibition studies. After pre-incubation, SLS-phage clone preparations (1.0×10^{11} pfu) in EBM-2 with or without vitronectin (20 μg/mL), fibrinogen (50 μg/mL), RGD (100 μM), holo-transferrin (100 μM), and monensin (2.5 μM) were added in the medium on the apical side, and the numbers of phage genome equivalents of the permeated SLS-phages on the basal side were determined by means of qPCR. For the *in vitro* monkey and rat BBB permeability assays, commercial BBB models (MBT-24H and RBT-24H, PharmaCo-Cell Company, Japan) were used.

Cell viability assay

hCMEC/D3 cells (1.0×10^4 cells per well) were seeded on a 96-well plate and cultured for 48 h. Then, the cells were incubated for 24 and 48 h with fresh EBM-2 containing cyclic SLS derivative (0–100 μM) at 37 °C. Cellular viability was measured with a Cell Counting Kit-8 (Dojindo, Kumamoto, Japan).

TEER assay

The hCMEC/D3 cell monolayers were prepared on 6-well Transwell plates. After pre-incubation in fresh EBM-2 for 10 min at 37 °C, the cyclic SLS derivative (0–100 μM) in EBM-2 was subjected to the medium on the apical side of the monolayer. The TEER value was determined at discrete timepoints during incubation at 37 °C.

Cellular uptake assay

hCMEC/D3 cells (5.0×10^4 cells per well) were seeded onto 24-well plates and cultured for 48 h. hCMEC/D3 cells were pre-incubated with fresh EBM-2 at either 37 °C or 4 °C for 10 min, and then the SLS-phages clone preparation (1.0×10^{11} pfu) or the fluorescent SLS peptide (10 μM) in EBM-2 were added. After incubation for discrete periods at the same temperature, the internalized SLS-phages or fluorescent SLS derivative were extracted using 1% Triton-X and quantified by plaque assay or fluorescent plate reader, respectively (Tecan infinite M1000, Tecan, Switzerland). In SLS-phage uptake inhibition study, cyclic SLS derivative (10 μM) or a macropinocytosis inhibitor EIPA (100 μM; Cayman Chemical) were added during pre-incubation and internalizing. Intracellular SLS-phage was visualized by immunostaining as described in the immunostaining section after the uptake assay in the 8-well chamber slide. The fluorescent signals were observed by confocal microscopy (TCS SP5, Leica Microsystems, Wetzlar, Germany). The internalization of fluorescent SLS peptide was also monitored by confocal microscopy.

***In vivo* BBB permeability assay**

ICR mice (male, 7–10 weeks old) were obtained from Kyudo (Saga, Japan). All mice were maintained in a room with controlled temperature (18–24 °C) and a 12 h light/dark cycle. Mice were given *ad libitum* access to food and water. The phage clone preparation (1.0×10^{11} pfu) was injected into the jugular vein, and the mice were kept at 37 °C on a hot plate. Following blood sampling (100 μL) after 60 min, cold PBS was perfused for 5 min via cardiac perfusion to wash out the phages that were non-specifically bound to the surface of vascular endothelial cells in the brain. The whole brain was isolated and homogenized using a Micro Smash MS-100R (Tomy Seiko, Tokyo, Japan). Brain homogenate was centrifuged

at 20,000 *g* for 30 min, and the supernatant was recovered as brain fraction. The phage titers in plasma and brain fraction were determined by plaque formation assay. All animal experiments were approved by the Institutional Animal Care and Use Committee of Kumamoto University, and the experiments were conducted in accordance with the regulations for animal experiments in Kumamoto University.

Immunostaining

After performing the cold PBS perfusion *in vivo* BBB permeability assay as described above, 4% paraformaldehyde (PFA) was perfused for 5 min to prefix the brain. The whole brain was isolated and incubated in 4% PFA for 24 h at 4 °C. The fixed brain was dehydrated with 30% sucrose for 24 h at 4 °C, then frozen and stored at −80 °C until sectioning; 20 μm brain slices were prepared using the standard method [44]. Brain slices were incubated in 0.3% Triton-X for 10 min and in blocking solution containing 2% donkey serum, 1% BSA, and 0.3% Triton-X in PBS for 2 h prior to overnight incubation with primary anti-m13+fd bacteriophage coat protein antibody (1:100; Abcam, ab6188) at 4 °C. DyLight 488 labeled-secondary antibody (1:100; Abcam, ab150081) and DyLight 594 labeled *Lycopersicon esculentum* (Tomato) lectin (1:100; Vector Laboratories, DL-1177) were added for 2 h at room temperature. Nuclei were stained with VECTASHIELD® Mounting Medium containing DAPI. Then, the brain slices were observed by confocal microscopy.

For hCMEC/D3 cells, the cells were seeded with a density of 2.0×10^4 cells in each well on 8-well chamber slides and cultured for 24 h. After pre-incubation with fresh EBM-2 at 37 °C for 10 min, hCMEC/D3 cells were incubated with EBM-2 containing SLS-phage (1.0×10^{11} pfu) for 10 min. Then, hCMEC/D3 cells were washed with cold PBS four times and incubated with 4% PFA for 10 min at room temperature. The surface of hCMEC/D3 cells was permeabilized with 0.1% Triton-X and blocked with 1% bovine serum protein solution. The internalized SLS-phage was detected by the primary anti-m13+fd bacteriophage coat protein antibody (1:100; Abcam, ab6188) and goat anti-rabbit IgG H and L (Alexa Fluor 568) preabsorbed (1:1,000; Abcam, ab175695), as described above.

Liposome study

Fluorescent DiO-labeled liposomes were synthesized by the thin-film hydration method. A total of 300 nmol lipids (COATSOME NC-50/cholesterol = 7:3 molar ratio) and fluorescent DiO (15 nmol) were dissolved in 600 μL chloroform, and then the solution was evaporated by vacuum centrifugation. The dry lipid film was hydrated using 10 mM HEPES buffer for 10 min. The sample was sonicated in a bath-type sonicator (ULTRA SONIC CLEANER AU-12C) to form control liposomes. SLS-STR modified liposomes (SLS-liposomes) were prepared by mixing control liposomes with SLS-STR peptide (10:1 molar ratio). The size and zeta potential of prepared liposomes were measured using a ZETASIZER NANO instrument (Malvern Panalytical Ltd, UK). The synthesized liposomes were diluted with EBM-2 to obtain preparations containing 0.1 mM liposome and 10 μM DiO, which were used in the uptake and permeability assays. In the animal study, the DiO-labeled liposome preparation (50 nmol liposome, 5 nmol DiO) was injected into the mouse jugular vein. After maintaining the mice for 1 h, the plasma, brain, spleen, liver and kidney were recovered as described above. Liposome quantities were determined using a fluorescent plate reader, as described above.

Statistical analysis

All experimental values are presented as the mean ± SEM, and Graph Pad Prism 7 (GraphPad Software, San Diego, USA) was used for the statistical analyses. To assess the significance of the differences between the means of two groups, the unpaired, two-tailed Student's t-test was conducted. Among the means of more than two groups, one-way analysis of variance

followed by Tukey's test was conducted to determine the significance of the differences. The criterion of statistical significance was set as $p < 0.05$.

4. Results

Identification of cyclic peptides improving permeation of the phage across the hCMEC/D3 cell monolayer

A phage library estimated to display 10^9 cyclic heptapeptides was screened using the hCMEC/D3 cell permeability assay to identify cyclic peptides that improve the permeation of phages across the human BBB (Fig. 1A). Moreover, because interactions between the carrier molecules and serum proteins can potentially inhibit BBB permeation [45, 46], the phage library was screened in the culture medium containing 5% FBS to ensure that positive screen hits are not affected by serum proteins.

In screening round 1, the original library (1.0×10^{11} pfu) in the medium was added on the apical side (luminal side) of the hCMEC/D3 cell monolayer. The phages permeated on the basal side (abluminal side) were enumerated by plaque assay. Permeated phages were detectable after 1 min, and their number was increased until 60 min (Fig. 1B). The permeated phages were amplified to create a second phage library that was screened another two times using the same hCMEC/D3 permeability assay.

During the 2nd screening, the number of permeated phages increased up to 10 min (Fig. 1B), and those phages were amplified for further screening. During the 3rd screening round, the number of permeated phages increased from 1 to 10 min (Fig. 1B). Between the 2nd and 3rd screening, there was no difference in the number of phages that permeated time-dependently. According to the manufacturer's protocol, the target phage clones were expected to be selected after the 3rd screening. Thus, we terminated the phage library screening after the 3rd round.

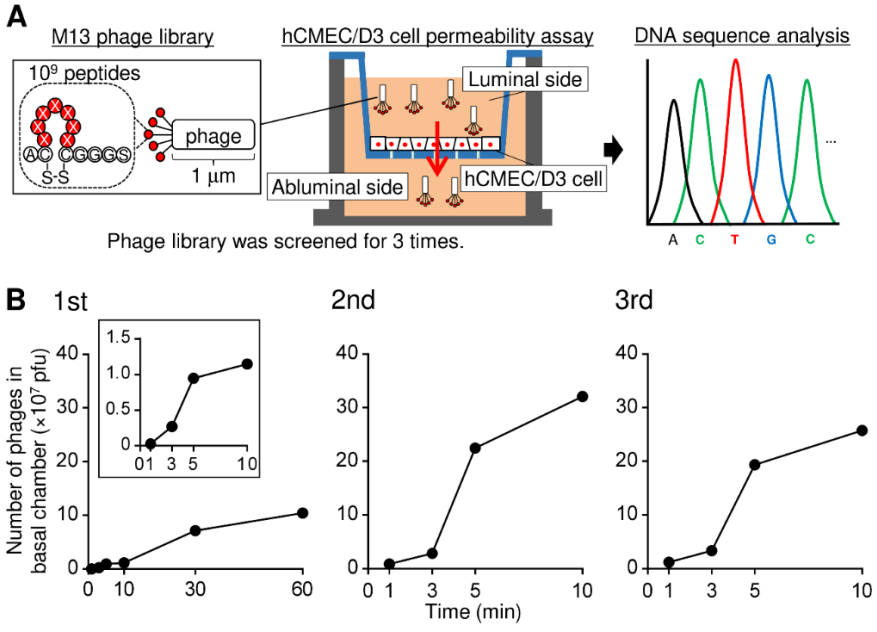

Fig. 1 Phage library screening with the hCMEC/D3 cell permeability assay.
(A) Schematic representation of the screening for BBB-permeable cyclic heptapeptides. The phage library was screened three times with the permeability assay with hCMEC/D3 cell monolayer. In the first round, the original library in the medium was added on the apical side (1.0×10^{11} pfu). The phages, which permeated across the cell monolayer, were collected from the basal side. The permeated phages were used as a prescreened library in the next round. The plaques from selected phages were randomly selected for DNA sequencing. (B) Time

course of phage permeation to the basal side during the 1st, 2nd, and 3rd round of screening. The numbers of phages were determined by plaque assay.

In screening round 3, 87 and 86 phage clones were randomly selected from phages that permeated during the periods of 0–1 min and 3–5 min, respectively, and DNA sequence analysis identified 170 unique cyclic heptapeptides (Tables 1 and S1), but the sequences SLSHSPQ (SLS) and NTGSPYE (NTG) were identified in 2 and 3 clones, respectively. The cyclic SLS peptide had a neutral isoelectric point (pI, 6.99), and NTG was anionic (pI, 3.00). The heptapeptide SLSHSPQ closely resembled an amino acid sequence in mouse vitronectin, except for the P residue (UniProtKB: P29788.2; SLSHSAQ, amino acid positions 358–364). Cyclic peptide NTGSPYE did not match any blood protein sequences or peptide binding sites within certain receptors. Further experiments were conducted with these two candidates.

Table 1 Amino acid sequences of the identified cyclic peptides and their isoelectric points.

Phage clone	Sequence	Frequency	Isoelectric point
SLS	C-SLSHSPQ-C	2/93	6.99
NTG	C-NTGSPYE-C	3/93	3.00

The indicated amino acids sequences were identified in more than a single clone. Unique sequences present in single clones are summarized in supplemental information (Table S1). The estimated isoelectric point was calculated using GENETYX Ver.11 (GENETYX, Tokyo, Japan).

Permeation of the identified phage clones across the hCMEC/D3 cell monolayer

To evaluate the facilitation of the phage permeation across the hCMEC/D3 cell monolayer by the identified cyclic peptides, the phage clones displaying SLSHSPQ and NTGSPYE (SLS-phage and NTG-phage, respectively) were examined in the hCMEC/D3 cell permeability assay in comparison with a control phage lacking a cyclic peptide. Phages with the cyclic peptides permeated to the basal side within 1 min, and their number increased time-dependently until 30 min (Fig. 2A). The numbers of permeated SLS-phages and NTG-phages were significantly higher than those of the control phages by 3.34- and 3.67-fold at 30 min, respectively (Fig. 2A). The results suggested that both identified cyclic peptides promoted phage permeation across the hCMEC/D3 cell monolayer.

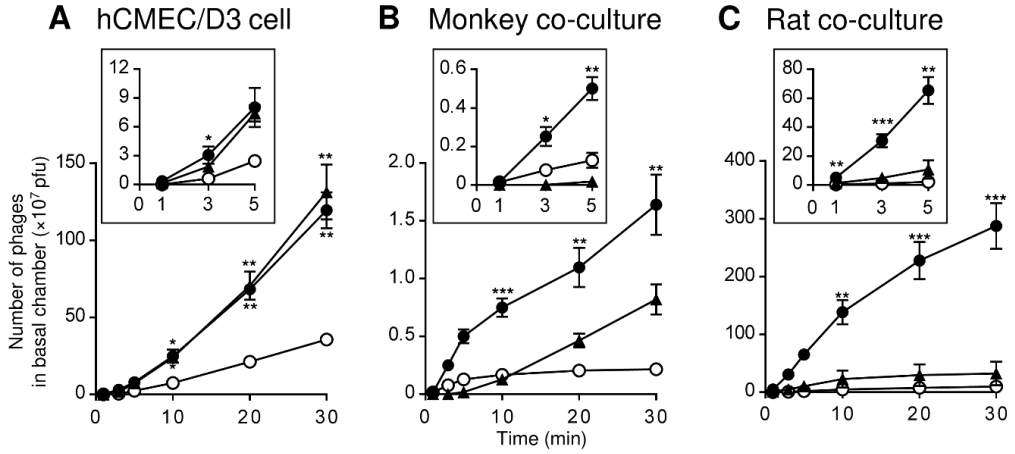

Fig. 2 Permeability assay with identified clones from phages that crossed the hCMEC/D3 cell monolayer, as well as the *in vitro* monkey and rat co-culture BBB models.

(A-C) The BBB permeation of two identified phage clones (1.0×10^{11} pfu) was tested with the permeability assay using the *in vitro* human (A, hCMEC/D3 cell), monkey (B, co-culture), and rat BBB models (C, co-culture). The numbers of phages permeated on the basal side were measured by means of qPCR. Closed circle, SLS-phage; closed triangle, NTG-phage; open circle, control phage. Each data point represents the mean ± SEM (n = 3). $^{*}p < 0.05$, $^{**}p < 0.01$, $^{***}p < 0.005$, significantly different from control phages.

Permeation of SLS- phages across monkey and rat BBB co-culture models *in vitro*

To examine whether BBB permeation by two identified cyclic peptides depends on the species, we performed permeability assays using monkey and rat BBB co-culture models consisting of primary brain microvascular endothelial cells, pericytes, and astrocytes. Both the monkey and rat BBB co-culture models had higher transepithelial electrical resistance (TEER) values (approximately 400 and 300 Ω×cm^2, respectively), an index of tight-junction integrity, than the hCMEC/D3 cell monolayer (approximately 100 - 150 Ω×cm^2). As shown in Fig. 2B and C, at 30 min, there were significantly more, i.e., 7.63- and 28.3-fold more, permeated SLS-phages than control phages in the monkey and rat BBB co-culture models, respectively. In contrast, the numbers of permeated NTG-phages did not significantly differ from the control phage numbers in the monkey and rat BBB co-culture models (Fig. 2B and C). These results indicated that the SLS peptide promoted phage permeation in monkey and rat BBB co-culture models *in vitro*. Therefore, in the next experiments, we focused on the cyclic SLS peptide.

The effect of a synthetic cyclic SLS derivative on viability and tight-junction integrity in hCMEC/D3 cells

To assess the possibility that the cyclic SLS peptide facilitates paracellular diffusion due to cytotoxicity or reducing tight-junction integrity, we examined the effects of a synthetic cyclic SLS derivative conjugated with a GGGS linker (AC-SLSHSPQ-CGGGS) on viability and tight-junction integrity in hCMEC/D3 cells. The viability of peptide-treated cells was not affected at the highest concentration (100 μM) for up to 48 h, similar to that of non-treated cells (Fig. 3A). Furthermore, incubation with up to 100 μM cyclic SLS derivative for 48 h did not decrease the TEER value of the cell monolayer, compared to that of the non-treated cell monolayer (Fig. 3B). These results suggested that the cyclic SLS peptide did not facilitate the paracellular diffusion of phages.

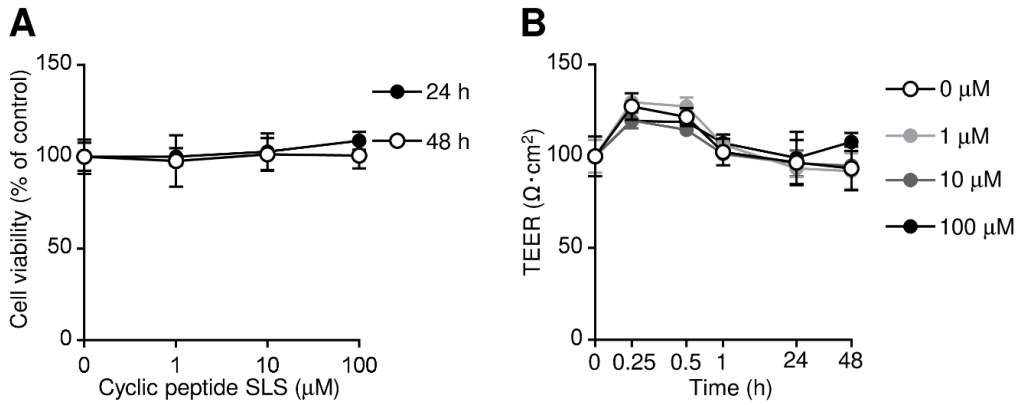

Fig. 3 The effect of synthetic cyclic SLS derivative on viability and tight-junction integrity of hCMEC/D3 cells.

(A) hCMEC/D3 cells were incubated with synthetic cyclic SLS derivative for 24 h (circle) or 48 h (square) at indicated concentrations (0–100 μM). Cell viabilities were measured using the cell counting kit-8. Each data point represents the mean ± SEM (n = 6). (B) Effect of the synthetic cyclic SLS derivative on the tight-junction integrity of the hCMEC/D3 cell monolayer. hCMEC/D3 cells were treated with SLS derivative (0–100 μM). After incubation for 48 h, TEER values were measured at each timepoint. Each data point represents the mean ± SEM (n = 3). Both the TEER and cell viability values did not significantly differ among the various SLS peptide concentrations at the indicated timepoints ($p > 0.05$).

The mechanism of transcellular permeation of SLS-phages in hCMEC/D3 cells

Internalization is the first step of the transcellular permeation. Therefore, the internalization of SLS-phages into hCMEC/D3 cells was evaluated by immunostaining as evidence of transcellular permeation. As shown in Fig. 4A, after incubation for 10 min, SLS-phages were detected around the nuclei, whereas control phages were not detected. This result indicated that the cyclic SLS peptide facilitated internalization of phages into hCMEC/D3 cells. Then, the competitive inhibitory effect of the synthetic cyclic SLS derivative on SLS-phage internalization into hCMEC/D3 cells was examined to elucidate the involvement of the cyclic SLS peptide in facilitating BBB permeation. As shown in Fig. 4B, co-incubation with the synthetic cyclic SLS derivative significantly reduced SLS-phage internalization by 67.4%, and the reduced internalization was at the same level as that of the control phage. In addition, at 4 °C, the internalization was also significantly reduced by 70.0%, indicating that SLS-phage internalization is an SLS peptide-mediated and energy-dependent process, possibly a receptor-mediated pathway.

Since the M13 phage is approximately 1 μm long, we hypothesized that the SLS-phage is internalized into the cells via macropinocytosis, because macropinosomes have a size of approximately 5 μm. As shown in Fig. 4B, EIPA (a macropinocytosis inhibitor) reduced SLS-phage internalization into hCMEC/D3 cells by 73.9%, resulting in a similar level to that of the control phage. This suggests that SLS-phage internalization involves receptor-mediated macropinocytosis.

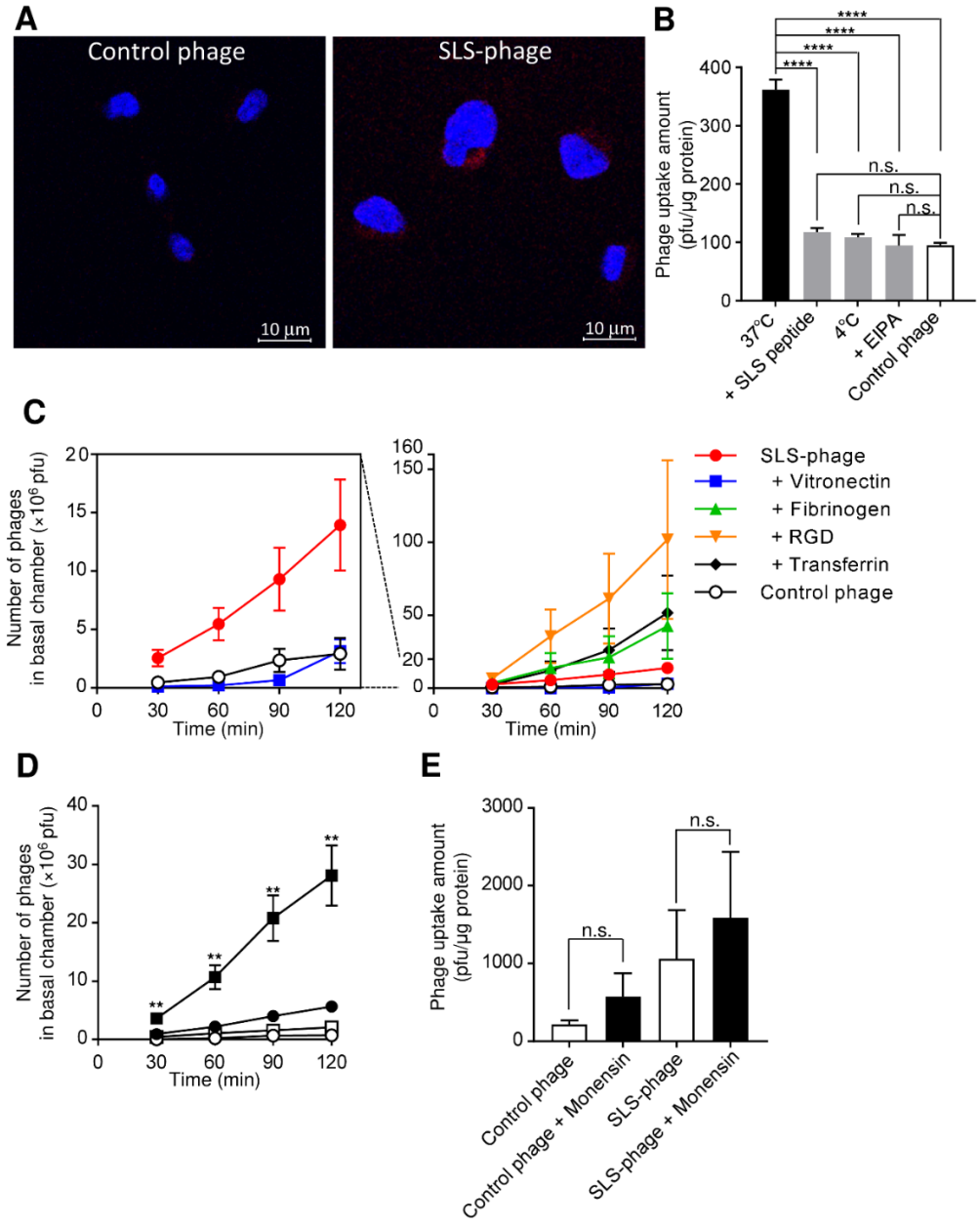

Fig. 4 Characterization of transcellular permeation of SLS-phages across hCMEC/D3 cell monolayer.

(A) Confocal fluorescence microscopic images of SLS-phages internalized into hCMEC/D3 cells. hCMEC/D3 cells were incubated with SLS-phages (1.0×10^{11} pfu) for 10 min at 37 °C. Internalized SLS-phages were visualized by immunostaining (phage, green; nuclei, blue). (B) Effect of low temperature, synthetic cyclic SLS derivative, and EIPA (macropinocytosis inhibitor) on the uptake of SLS-phage by hCMEC/D3 cells. Each data point represents the mean ± SEM (n = 3). ****$p < 0.001$, significantly different. (C) Effect of human integrin ligands and holo-transferrin on SLS-phage permeation across hCMEC/D3 cell monolayer (closed circle, SLS-phage; closed square, SLS-phage + Vitronectin; closed triangle, SLS-phage + Fibrinogen; inverted triangle, SLS-phage + RGD; closed diamond, SLS-phage + holo-transferrin; open circle, control phage). The Left graph is a magnified graph with a range from 0 to 20 x 10^6 pfu in the right graph. ANOVA did not detect significant differences among the conditions ($p > 0.05$). (D) Effect of monensin on the permeation of SLS-phages and control phages across the hCMEC/D3 cell monolayer (closed circle, SLS-phage; closed diamond, SLS-phage + Monensin; open circle, control phage; open diamond, control phage

+ Monensin). Each data point represents mean ± SEM (n = 3). $^{**}p < 0.01$, significantly different from SLS-phages. (E) Intracellular titers of SLS-phages and control phages in hCMEC/D3 cell monolayer at 120 min with or without monensin treatment. (F) Hypothesis of the mechanism of SLS-phage permeation across the hCMEC/D3 cell monolayer.

Effects of vitronectin, fibrinogen, and RGD peptide on SLS-phage permeation

The heptapeptide SLSHSPQ matches an amino acid sequence segment in mouse vitronectin (amino acid residue positions 358–364), except for the P residue, and its N-terminal SLS motif is also conserved in human vitronectin (amino acid residue positions 297–299). Vitronectin is a ligand for integrin family receptors, and integrins are internalized into cells via macropinocytosis [47-49]. Therefore, we hypothesized that SLS-phages permeate across the hCMEC/D3 cell monolayer via the vitronectin receptor. To test this hypothesis, the inhibitory effects of human vitronectin and two other integrin ligands, RGD peptide and human fibrinogen, on the permeation of SLS-phages across the hCMEC/D3 cell monolayer were examined. Competition by human holo-transferrin was also assessed to test the possible involvement of the transferrin receptor in SLS-phage permeation. By co-incubation with vitronectin, the SLS-phage counts on the basal side were decreased by 77.4% at 120 min to levels that were similar to those of the control phages (Fig. 4C). This result suggested that the SLS-phage permeation across the hCMEC/D3 cell monolayer involves the vitronectin receptor. Interestingly, the RGD peptide, fibrinogen, and holo-transferrin enhanced the permeation of SLS-phages by 7.30-, 3.06-, and 3.70-fold at 120 min, respectively (Fig. 4C). This result suggested that SLS-phage permeation is induced by the holo-transferrin receptor and integrin ligands, except vitronectin.

The enhancing effect of monensin on SLS-phage permeation

Transferrin is a booster for exosome release [50], and it has been reported that integrin family proteins are secreted from the intracellular space as exosomes. Therefore, we hypothesized that the exosome system is involved in the secretion of SLS-phages from hCMEC/D3 cells. To examine this hypothesis, the effect of monensin, another booster for exosome release, on SLS-phage permeation across the hCMEC/D3 cell monolayer was investigated. By co-incubation with monensin, the number of SLS-phages on the basal side was significantly increased by 4.93-fold at 120 min, whereas that of control phages was not affected (Fig. 4D). At 120 min, the intracellular phage titer was not significantly increased by monensin treatment (Fig. 4E). This result suggested that monensin treatment induced both the internalizing and the externalizing processes of the SLS-phage.

Permeation of SLS-phages across the mouse BBB *in vivo*

To examine whether SLS-phages permeate across the mouse BBB *in vivo*, we quantified the SLS-phages in the brain and plasma by plaque assay after intravenous (i.v.) administration. As shown in Fig. 5A, in the brain, the SLS-phage titer was 12.8-fold higher than the control phage titer at 60 min after the administration, whereas the plasma concentration of the SLS-phage did not differ from that of the control phage. In addition, we conducted immunostaining of mouse brain slices to monitor the distribution of the SLS-phages into the brain parenchyma. At 60 min after i.v. administration, SLS-phages were detected as dot-like signals from around the brain microvessels in the cerebral cortex and hippocampus, and a proportion of those diffused into the brain parenchyma (Fig. 5B). Therefore, the quantity of SLS-phages in the brain shown in Fig 5A is suggested to mainly reflect the amount in the brain parenchyma. Control phages were not detected around the brain microvessels in the cerebral cortex or hippocampus. These results indicated that cyclic SLS peptide facilitated phage permeation across the mouse BBB *in vivo*.

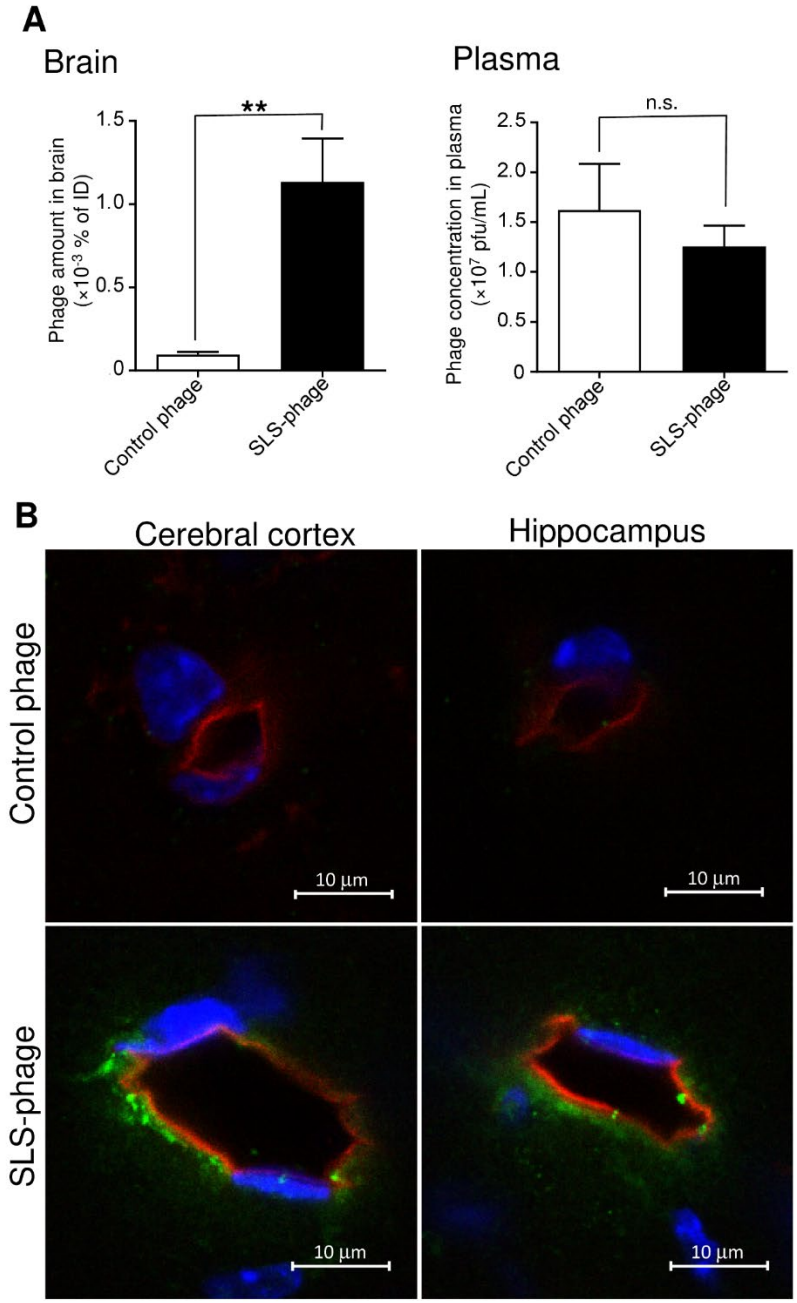

Fig. 5 Distribution of SLS-phages in the mouse brain *in vivo* after intravenous administration.

(A) SLS-phages or control phages (1.0×10^{11} pfu) were administered by i.v. injection, blood was collected, and the brain was excised 60 min post-injection. Plaque assay was performed to determine the phage numbers in the brain and plasma fraction. Each data point represents the mean ± SEM (n = 5–6). $^{**}p < 0.01$, significantly different. (B) Phages in the cerebral cortex and hippocampus section were detected by immunostaining (phage, green; blood vessel, red; nuclei, blue).

Internalization of synthetic FAM-labeled SLS derivative in hCMEC/D3 cells

The transcellular permeability assay using hCMEC/D3 cell monolayers is not considered an appropriate test for examining the permeation of small molecules, such as SLS-FAM and FAM, because the contribution of paracellular diffusion could be larger than that of transcellular permeation. Therefore, we initially examined whether a synthetic FAM-labeled

SLS derivative (SLS-FAM, Mw: 1774) internalizes into hCMEC/D3 cells as the first step of transcellular permeation to test the possibility that the synthetic SLS peptide permeates across the BBB similar to the SLS-phage. As shown in Fig. 6A, the intracellular fluorescence signal of SLS-FAM was greater than that of the fluorescent dye FAM alone (Mw: 376) from 5 to 30 min after assay initiation (Fig. 6A). Moreover, SLS-FAM was detected in the cytosol at 5 min by confocal laser scanning microscopy, whereas FAM alone was not detected (Fig. 6B). These results indicated that the synthetic cyclic SLS derivative could internalize into the hCMEC/D3 cells similar to the SLS-phage.

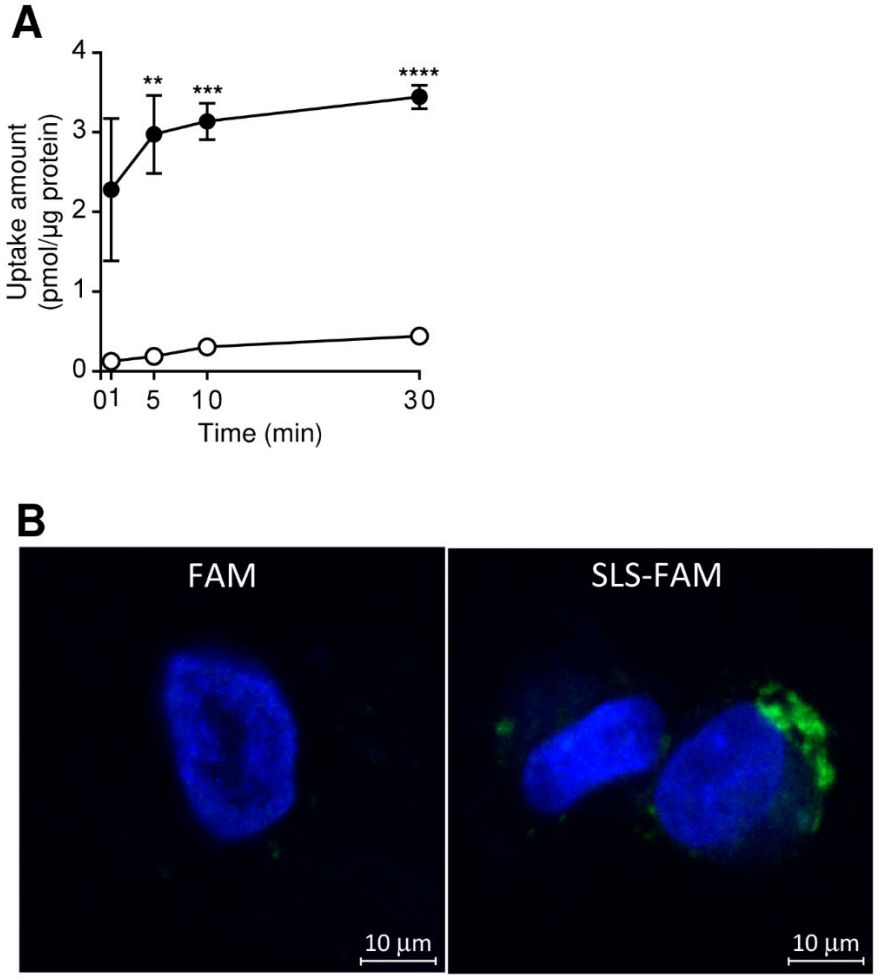

Fig. 6 Internalization of FAM-labeled SLS derivative into hCMEC/D3 cells.
(A) Time course of SLS-FAM (10 μM) and FAM (10 μM) uptake by hCMEC/D3 cells (closed circle, SLS-FAM; open circle, FAM). Each data point represents mean ± SEM (n = 3). $^{**}p < 0.01$, $^{***}p < 0.005$, $^{****}p < 0.001$ significantly different from FAM. (B) Confocal fluorescence microscopic images of internalization of SLS-FAM in hCMEC/D3 cells. hCMEC/D3 cells were incubated with SLS-FAM (10 mM) for 5 min at 37 °C. FAM, green; nuclei, blue.

Permeation of cyclic SLS peptide-coated liposomes across the BBB cell monolayer models

The nanocarrier transport activity of the cyclic SLS peptide was investigated using liposomes. The liposomes coated with SLS peptide at a molar ratio of 1% or 10% were constructed (1%-SLS-liposome or 10%-SLS-liposome). The prepared liposomes had a size of approximately

150 nm with a monodisperse distribution and a zeta potential of approximately -44 mV (Table 2).

Table 2 The size and zeta potential of prepared liposomes.

Liposome preparation	Size (nm)	Polydispersity index	Zeta potential (mV)
Control liposomes	149 ± 3	0.235 ± 0.004	-43.9 ± 0.5
1%-SLS-liposomes	155 ± 5	0.249 ± 0.001	-46.1 ± 0.2
10%-SLS-liposomes	152 ± 2	0.243 ± 0.004	-41.9 ± 0.2

Each liposome preparation was made using the thin-film hydration method. The size and zeta potential were measured with a ZETASIZER NANO instrument. Each data point represents the mean ± SEM (n = 3).

Initially, the internalization of SLS-liposomes into hCMEC/D3 cells was investigated. As shown in Fig. 7A, the intracellular amount of the 10%-SLS-liposomes was time-dependently increased during incubation for up to 30 min, and at 5 min the intracellular amount of 10%-SLS-liposomes was 17.8-fold greater than that of control liposomes. This observation indicated that the SLS-peptide facilitated the internalization of liposomes into hCMEC/D3 cells.

Then, the permeation of SLS-liposomes across the hCMEC/D3 cell monolayer was examined (Fig. 7B). On the basal side at 30 min, the amount of 10%-SLS-liposomes was 1.23-fold higher than that of control liposomes. Moreover, the 1%-SLS-liposomes also permeated across hCMEC/D3 cell monolayer, and their permeability was on the same level as the 10%-SLS-liposomes. However, the differences in the permeability between SLS-liposomes and control liposomes were smaller than those in the phage experiments. This is likely due to the high rate of paracellular diffusion compared with transcellular permeability because the sizes of liposomes are smaller than phages (150 nm vs. 1 μm) and tight junction integrity in hCMEC/D3 cells was lower than co-culture models as mentioned in Fig. 2. Therefore, to decrease the contribution of paracellular diffusion to the permeation, we further investigated the permeability of SLS-liposomes using monkey and rat BBB co-culture models *in vitro*, which exhibited higher TEER values than hCMEC/D3 cells. On the basal side in the monkey and the rat model, there were 3.42-fold and 3.35-fold more 10%-SLS-liposomes than control liposomes at 30 min, respectively (Fig. 7C and D). Moreover, the 10%-SLS-liposomes showed a higher BBB-permeability than the 1%-SLS-liposomes. These results indicated that the cyclic SLS peptide also facilitated the *in vitro* BBB permeability of liposomes by surface modification.

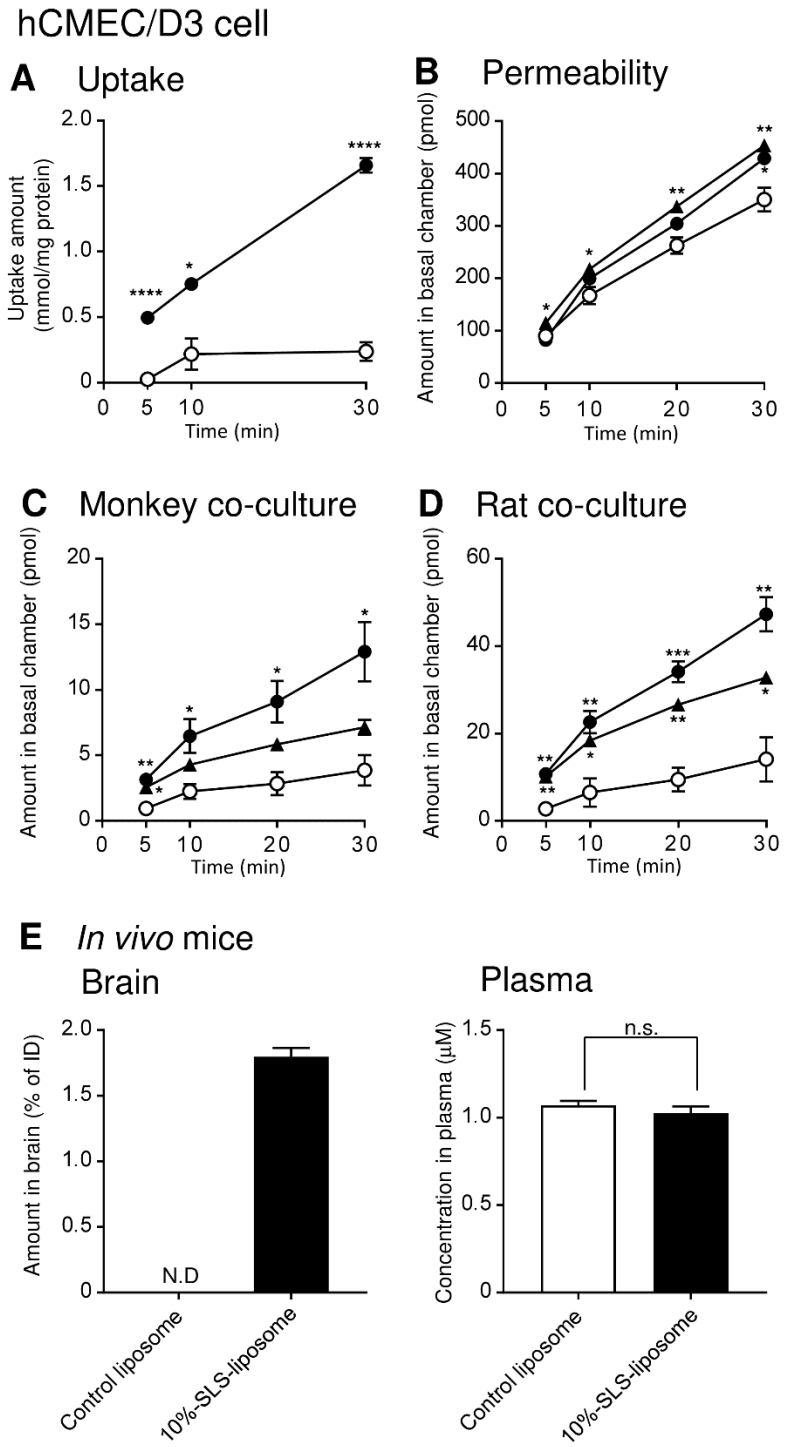

Fig. 7 Permeation of SLS-liposomes across the BBB *in vitro* and *in vivo*.
(A) Time course of 10%-SLS-liposome and control liposome uptake by hCMEC/D3 cells. Each liposome was labeled with fluorescent DiO, and the proportion of liposome uptake was determined by a fluorescent plate reader. (B-D) SLS-liposome and control liposome permeation across the *in vitro* human (B, hCMEC/D3 cell), monkey (C, co-culture), and rat BBB models (D, co-culture). Closed circle, 10%-SLS-liposome; closed triangle, 1%-SLS-liposome; open circle, control liposome. (E) During the *in vivo* study, the content of each liposome in the brain and plasma was determined at 1 h after i.v. administration into the mice. Each data point represents the mean ± SEM (n = 3). *$p < 0.05$, **$p < 0.01$, ***$p < 0.005$, ****$p < 0.001$ significantly different from control liposomes.

Permeation of SLS-liposomes across the mouse BBB *in vivo*

To examine whether 10%-SLS-liposomes permeate across the mouse BBB *in vivo*, we measured the amount of 10%-SLS-liposome in the brain and plasma after i.v. administration. As shown in Fig. 7E, the content of 10%-SLS-liposome in the brain was 1.80% of injected dose (599 pmol/g brain), but that of the control liposome was below the limit of detection at 60 min after the i.v. administration. The plasma concentration of 10%-SLS-liposomes did not differ from that of control liposomes (Fig. 7E). These results demonstrated that the cyclic SLS peptide facilitated liposome permeation across the mouse BBB *in vivo*. In addition, there was not a significant difference between the amount of 10%-SLS-liposome and control liposome in the liver and the spleen (Fig. S1). The amounts of both liposomes in the kidney was under the detection limit.

5. Discussion

We identified the neutral, BBB-permeable cyclic SLS heptapeptide for brain delivery of macromolecules via macropinocytosis and the exosome secretion pathway. Cationic CPPs typically diffuse to the cytosolic space and are trapped in intracellular organelles after macropinocytosis-mediated internalization because of electrostatic interactions between cationic CPPs and the anionic macropinosome membrane [34-36]. In contrast, the neutral cyclic SLS peptide facilitated phage permeation across the hCMEC/D3 cell monolayer via macropinocytosis. Therefore, there was the possibility that the cyclic SLS peptide was not diffused to the intracellular compartment but was transcytosed to the brain parenchyma (Fig. 4F).

The nanoparticle size is critical for BBB permeability. In current drug delivery systems, the nanoparticle size is approximately 100–200 nm [51]. However, silica-nanoparticles of 100 nm or larger could not permeate across primary rat BBB *in vitro* [45]. Moreover, PEI modified cationic beads (500 nm) did not permeate across hCMEC/D3 cell monolayers, although these beads were internalized via macropinocytosis. As described above, cationic compounds are typically diffused to the cytosolic space and trapped in intracellular organelles. Even if the size of nanoparticle is less than 50 nm, Qdots cannot permeate across the primary rat BBB *in vitro* using 2% FBS buffer because of the formation of a "protein corona" between the nanoparticles and serum proteins [45, 46]. In this study, we screened a phage library (average phage particle size: 1 μm) in the presence of 5% FBS. We identified the cyclic SLS peptide that improved the BBB permeability of phages and liposomes (average size: 150 nm) in reconstituted BBB cell culture models used in the presence of 5% FBS and even in mice after i.v. administration (Figs. 2, 5, and 7; Table 2). Cationic carriers have been reported to aggregate in the blood and increase in size at the micrometer level because of electrostatic interactions with serum proteins. The cyclic SLS peptide was neutral in the blood, and therefore, less likely to form a protein corona than cationic carriers. Thus, using the cyclic SLS peptide in nanoparticles for drug delivery could overcome the size limitation and the effect of serum proteins commonly associated with this type of drug delivery system.

The size of liposomes in the present study was approximately 150 nm (Table 2), which is larger than the size of clathrin or caveolae-mediated endosomes (50-100 nm). Therefore, it is possible that macropinocytosis is also involved in the permeation of SLS-liposomes as well as phages, although the involvement of another transport mechanism cannot be ruled out. In terms of transport direction, it is a possibility that the cyclic SLS peptide functions for brain-to-blood transport. The SLS-phage and SLS-liposome were accumulated in mouse brain at 60 min after i.v. administration (Fig. 5 and 7E), suggesting that the blood-to-brain transport is dominant to the opposite transport for the cyclic SLS peptide. Further studies are necessary to clarify the detail transport mechanism of the cyclic SLS peptide.

Kozlovska and Stepensky summarized the percent of injected dose of brain targeted vesicles [52]. The geometric mean was 0.23% of injected dose and 8 vesicle-based DDS showed greater than 1% of injected dose out of 35 reports. For example, transferrin-conjugated nanoparticles of poly(lactide)-D-α-tocopheryl polyethylene glycol succinate (PLA-TPGS) diblock copolymer was distributed to the rat brain with 1.1% of injected dose at 4h after administration [53]. As peptide carriers, angiopep-2-conjugated biodegradable polymersomes penetrated 0.1% of the injected dose in rat brain at 24 h [54]. As shown in Fig 7E, 1.8% of injected 10%-SLS-liposome was detected in mouse brain at 60 min after i.v. administration. Although the experimental conditions were different among reports, it is possible that the brain distribution of SLS-liposomes is not inferior to the brain-targeted vesicles reported previously.

The percentage of the injected dose of SLS-liposome in the brain was 1586-fold greater than that of SLS-phages (Figs. 5A and 7E). A potential reason are differences in the size and displaying numbers of SLS-peptide between phages and liposomes. The M13 phage is about 1 μm in length, while the liposome is 150 nm in the diameter. Furthermore, 10%-SLS-liposome showed greater permeability than 1%-SLS-liposome across monkey and rat BBB co-culture models (Figs. 7C-D), suggesting that greater numbers of SLS-peptides increase the permeability of SLS-liposome across the BBB. The phage displays five cyclic peptides on one side of the phage particle. The larger size of phage particles and smaller number of SLS peptides are expected to lead to decreased efficiency of interactions with the surface receptor and internalization into the cells. In addition, the involvement of an unknown transport, other than macropinocytosis or clathrin- or caveola-mediated endocytosis, should also be considered.

The 10%-SLS-liposome also distributed into the reticuloendothelial systems (RES), including the spleen and liver, and those distributions were not significantly different from control liposome (Fig. S1). Additionally, the SLS- and control liposome were not detected in the kidney. Those results suggest that SLS peptides did not facilitate distribution into the spleen, liver and kidney, and the distribution into the spleen and liver was attributed to the property of liposomes. Indeed, the liposome tend to be accumulated in RES [55]. It was reported that PEGylation reduced distribution of liposomes into RES [56]. Thus, PEGylation is likely to be a rational strategy for further improvement of the brain distribution of SLS-liposomes by reducing their loss in RES, and the further studies, including distribution in the brain parenchyma, are necessary for application of the SLS-liposome for brain-targeted carriers.

Differences between species can have a large impact on translational research and clinical application. Recently, some clinical trials failed due to species differences in BBB. For example, cereport, a bradykinin analog, increased BBB permeability by transiently reducing tight-junction integrity and consequently improving brain delivery of the co-administrated anticancer drug in animal models. However, a clinical trial in glioma patients failed because there were differences in target protein expression, administration dose, and pharmacokinetics between animal models and humans [57]. Therefore, it is important that the BBB permeability is tested using human cell lines or several cell lines from different species during the early stage of carrier screening. In this study, the BBB permeability of the SLS-phage was investigated *in vitro* using a human (hCMEC/D3) cell monolayer model, along with a monkey and a rat BBB co-culture model, and *in vivo* using a mouse model. In all assays, the SLS-phages had a higher BBB permeability than the control phages (Figs. 2, 5). Moreover, the synthetic FAM-labeled SLS peptide was also internalized into hCMEC/D3 cells, and the SLS-liposomes permeated across the hCMEC/D3 cell monolayer, the *in vitro* monkey and rat BBB cell co-culture models, and the BBB in ICR mice (Figs. 6, 7). Therefore, we concluded that the permeability of the cyclic SLS peptide was not affected by species

differences in the BBB. In addition, the synthetic cyclic SLS peptide was not associated with *in vitro* cytotoxicity (Fig. 3). These results indicated that cyclic SLS peptide has properties suitable for applied studies using CNS disease animal models.

Interestingly, SLS-phage permeation across the hCMEC/D3 cell monolayer was stimulated by adding RGD, fibrinogen, and holo-transferrin (Fig. 4C). According to earlier reports, integrin family proteins are secreted with exosomes and transferred to other cells and tissues, and exosome secretion is promoted by holo-transferrin. Here we hypothesized that RGD and fibrinogen improved the BBB permeability of SLS-phages by activating exosome secretion via binding to integrin family receptors, except the vitronectin receptors. Indeed, monensin, an exosome secretion booster, significantly enhanced SLS-phage permeation (Fig. 4D and E), suggesting that the exosome system was involved in SLS-phage permeation. Recent results indicated that the exosome system is critically involved in cell-to-cell communication between the BBB and brain parenchyma [50]. We assumed that the SLS-phage was transferred from the BBB to brain parenchyma by exploiting endogenous exosome systems. Previous reports indicated that integrin adopts three conformational states: bent-closed inactive form, extended-closed intermediate-affinity state, and extended-open high-affinity state [58, 59]. Therefore, there was the possibility that RGD and fibrinogen facilitated the binding of cyclic SLS peptide to the vitronectin receptor site by changing the receptor conformation. It was considered that the human vitronectin interacted with integrins at both the RGD and SLS sites because the SLS-phage competed only with vitronectin. Thus, there was a possibility that the SLS residues are important for permeation across the BBB. Fibrinogen (200–400 mg/dL) and transferrin (200–300 mg/dL) are abundant proteins in human blood [60, 61]. This finding suggested the possibility that the cyclic SLS peptide can maintain the permeability even in the presence of 5% FBS and *in vivo* by coordination with serum integrin ligands and holo-transferrin (Figs. 4C, 5-7).

In other previous studies, BBB-permeable carriers were required for several hours or days to support permeation across the BBB. For example, the adenovirus (80–100 nm) and adeno-associated virus (AAV, 20–25 nm), particularly AAV9, have been reportedly used as BBB-permeable gene vectors [62, 63]. However, the BBB permeation required several hours *in vitro*, and AAV9 was trapped in astrocytes following permeation across the brain microvessel endothelial cells [64, 65]. SLS-phage permeation was detected at 1 min and 1 hour *in vitro* and *in vivo,* respectively (Figs. 2, 5). In addition, the SLS-phage permeated across the BBB co-culture models using astrocytes and pericytes (Fig. 2), and the M13 phage used in this study was larger than the adenovirus or AAV9. Therefore, we considered that the cyclic SLS peptide could quickly deliver the gene vectors to the brain parenchyma.

The phage therapy is expected to become an alternative treatment for antibiotics because it has a potent therapeutic effect against intractable infections and resistant microbes [66-68]. By using phages that specifically recognize pathogenic bacteria, phage therapy causes few or no side effects on host microbiota. In CNS diseases, the EC200^{pp}, an active phage against fatal neonatal meningitis, has been identified. However, it was reported that EC200^{pp} hardly distributed into the brain and cerebrospinal fluid compared with other tissues, such as kidney and spleen [69]. In this study, we demonstrated that the SLS-phage distributed to the brain parenchyma. Therefore, this finding could lead to novel phage therapy for CNS infections.

6. Conclusion

Our results demonstrate that the cyclic SLS peptide facilitates BBB permeation of M13 phages, the non-permeable compound FAM, and liposomes, indicating that it is a promising carrier candidate for macromolecular drugs and nanocarriers. In addition, peptide carriers are more useful than antibody carriers in terms of cost, synthesis, and immunogenicity. Therefore, the cyclic SLS peptide appears to be a potent tool for improving the brain delivery of

conjugated macromolecules and nanoparticles, enabling of development of novel CNS acting drugs and expanding the application of conventional drugs for CNS diseases.

7. Acknowledgments

This study was supported in part by AMED under Grant Number 18ak0101080, and JSPS KAKENHI Grant Number JP18H02590 and JP18J15384, JST CREST Grant Number JP171024167, and Mochida Memorial Foundation for Medical and Pharmaceutical Research.

8. Conflict of interests

The authors declare no conflict of interest.

9. References

[1] A. Akinleye, Z. Rasool, Immune checkpoint inhibitors of PD-L1 as cancer therapeutics. J Hematol Oncol. 12 (2019) 92, 10.1186/s13045-019-0779-5.

[2] B. Combadiere, M. Beaujean, C. Chaudesaigues, V. Vieillard, Peptide-Based Vaccination for Antibody Responses Against HIV. Vaccines (Basel). 7 (2019), 10.3390/vaccines7030105.

[3] A.A. Barba, S. Bochicchio, A. Dalmoro, G. Lamberti, Lipid Delivery Systems for Nucleic-Acid-Based-Drugs: From Production to Clinical Applications. Pharmaceutics. 11 (2019), 10.3390/pharmaceutics11080360.

[4] W.M. Pardridge, Why is the global CNS pharmaceutical market so under-penetrated?, Drug Discov Today. 7 (2002) 5-7.

[5] W.M. Pardridge, The blood-brain barrier: bottleneck in brain drug development. NeuroRx. 2 (2005) 3-14, 10.1602/neurorx.2.1.3.

[6] H.J. Lee, B. Engelhardt, J. Lesley, U. Bickel, W.M. Pardridge, Targeting rat anti-mouse transferrin receptor monoclonal antibodies through blood-brain barrier in mouse. J Pharmacol Exp Ther. 292 (2000) 1048-1052.

[7] W.M. Pardridge, Y.S. Kang, J.L. Buciak, J. Yang, Human insulin receptor monoclonal antibody undergoes high affinity binding to human brain capillaries in vitro and rapid transcytosis through the blood-brain barrier in vivo in the primate. Pharm Res. 12 (1995) 807-816, 10.1023/a:1016244500596.

[8] D. Wu, J. Yang, W.M. Pardridge, Drug targeting of a peptide radiopharmaceutical through the primate blood-brain barrier in vivo with a monoclonal antibody to the human insulin receptor. J Clin Invest. 100 (1997) 1804-1812, 10.1172/jci119708.

[9] K. Benchenane, V. Berezowski, C. Ali, M. Fernandez-Monreal, J.P. Lopez-Atalaya, J. Brillault, J. Chuquet, A. Nouvelot, E.T. MacKenzie, G. Bu, R. Cecchelli, O. Touzani, D. Vivien, Tissue-type plasminogen activator crosses the intact blood-brain barrier by low-density lipoprotein receptor-related protein-mediated transcytosis. Circulation. 111 (2005) 2241-2249, 10.1161/01.cir.0000163542.48611.a2.

[10] M. Demeule, J.C. Currie, Y. Bertrand, C. Che, T. Nguyen, A. Regina, R. Gabathuler, J.P. Castaigne, R. Beliveau, Involvement of the low-density lipoprotein receptor-related protein in the transcytosis of the brain delivery vector angiopep-2. J Neurochem. 106 (2008) 1534-1544, 10.1111/j.1471-4159.2008.05492.x.

[11] Y. Li, X. Zheng, M. Gong, J. Zhang, Delivery of a peptide-drug conjugate targeting the blood brain barrier improved the efficacy of paclitaxel against glioma. Oncotarget. 7 (2016) 79401-79407, 10.18632/oncotarget.12708.

[12] H. Hillaireau, P. Couvreur, Nanocarriers' entry into the cell: relevance to drug delivery. Cell Mol Life Sci. 66 (2009) 2873-2896, 10.1007/s00018-009-0053-z.

[13] I.D. Alves, C.Y. Jiao, S. Aubry, B. Aussedat, F. Burlina, G. Chassaing, S. Sagan, Cell biology meets biophysics to unveil the different mechanisms of penetratin internalization

in cells. Biochim Biophys Acta. 1798 (2010) 2231-2239, 10.1016/j.bbamem.2010.02.009.
[14] B. He, D. Yang, M. Qin, Y. Zhang, B. He, W. Dai, X. Wang, Q. Zhang, H. Zhang, C. Yin, Increased cellular uptake of peptide-modified PEGylated gold nanoparticles. Biochem Biophys Res Commun. 494 (2017) 339-345, 10.1016/j.bbrc.2017.10.026.
[15] A. Mishra, G.H. Lai, N.W. Schmidt, V.Z. Sun, A.R. Rodriguez, R. Tong, L. Tang, J. Cheng, T.J. Deming, D.T. Kamei, G.C. Wong, Translocation of HIV TAT peptide and analogues induced by multiplexed membrane and cytoskeletal interactions. Proc Natl Acad Sci U S A. 108 (2011) 16883-16888, 10.1073/pnas.1108795108.
[16] T. Asai, T. Tsuzuku, S. Takahashi, A. Okamoto, T. Dewa, M. Nango, K. Hyodo, H. Ishihara, H. Kikuchi, N. Oku, Cell-penetrating peptide-conjugated lipid nanoparticles for siRNA delivery. Biochem Biophys Res Commun. 444 (2014) 599-604, 10.1016/j.bbrc.2014.01.107.
[17] J.P. Lim, P.A. Gleeson, Macropinocytosis: an endocytic pathway for internalising large gulps. Immunol Cell Biol. 89 (2011) 836-843, 10.1038/icb.2011.20.
[18] N. Oh, J.H. Park, Endocytosis and exocytosis of nanoparticles in mammalian cells. Int J Nanomedicine. 9 Suppl 1 (2014) 51-63, 10.2147/ijn.s26592.
[19] G. Cao, W. Pei, H. Ge, Q. Liang, Y. Luo, F.R. Sharp, A. Lu, R. Ran, S.H. Graham, J. Chen, In Vivo Delivery of a Bcl-xL Fusion Protein Containing the TAT Protein Transduction Domain Protects against Ischemic Brain Injury and Neuronal Apoptosis. J Neurosci. 22 (2002) 5423-5431, 20026550.
[20] E. Kilic, G.P. Dietz, D.M. Hermann, M. Bahr, Intravenous TAT-Bcl-Xl is protective after middle cerebral artery occlusion in mice. Ann Neurol. 52 (2002) 617-622, 10.1002/ana.10356.
[21] U. Kilic, E. Kilic, G.P. Dietz, M. Bahr, Intravenous TAT-GDNF is protective after focal cerebral ischemia in mice. Stroke. 34 (2003) 1304-1310, 10.1161/01.str.0000066869.45310.50.
[22] W. Yin, G. Cao, M.J. Johnnides, A.P. Signore, Y. Luo, R.W. Hickey, J. Chen, TAT-mediated delivery of Bcl-xL protein is neuroprotective against neonatal hypoxic-ischemic brain injury via inhibition of caspases and AIF. Neurobiol Dis. 21 (2006) 358-371, 10.1016/j.nbd.2005.07.015.
[23] X.M. Liu, D.S. Pei, Q.H. Guan, Y.F. Sun, X.T. Wang, Q.X. Zhang, G.Y. Zhang, Neuroprotection of Tat-GluR6-9c against neuronal death induced by kainate in rat hippocampus via nuclear and non-nuclear pathways. J Biol Chem. 281 (2006) 17432-17445, 10.1074/jbc.M513490200.
[24] M.J. Simon, W.H. Kang, S. Gao, S. Banta, B. Morrison, 3rd, TAT is not capable of transcellular delivery across an intact endothelial monolayer in vitro. Ann Biomed Eng. 39 (2011) 394-401, 10.1007/s10439-010-0144-x.
[25] S. Patel, C.R. Leibrand, P. Palasuberniam, P.O. Couraud, B. Weksler, F.M. Jahr, J.L. McClay, K.F. Hauser, M. McRae, Effects of HIV-1 Tat and Methamphetamine on Blood-Brain Barrier Integrity and Function In Vitro. Antimicrob Agents Chemother. 61 (2017), 10.1128/aac.01307-17.
[26] F. Wang, Y. Wang, X. Zhang, W. Zhang, S. Guo, F. Jin, Recent progress of cell-penetrating peptides as new carriers for intracellular cargo delivery. J Control Release. 174 (2014) 126-136, 10.1016/j.jconrel.2013.11.020.
[27] C. Palm-Apergi, A. Lorents, K. Padari, M. Pooga, M. Hallbrink, The membrane repair response masks membrane disturbances caused by cell-penetrating peptide uptake. FASEB J. 23 (2009) 214-223, 10.1096/fj.08-110254.
[28] W.P. Verdurmen, R. Brock, Biological responses towards cationic peptides and drug carriers. Trends Pharmacol Sci. 32 (2011) 116-124, 10.1016/j.tips.2010.11.005.

[29] L.J. Arnold, Jr., A. Dagan, J. Gutheil, N.O. Kaplan, Antineoplastic activity of poly(L-lysine) with some ascites tumor cells. Proc Natl Acad Sci U S A. 76 (1979) 3246-3250, 10.1073/pnas.76.7.3246.
[30] S.W. Jones, R. Christison, K. Bundell, C.J. Voyce, S.M. Brockbank, P. Newham, M.A. Lindsay, Characterisation of cell-penetrating peptide-mediated peptide delivery. Br J Pharmacol. 145 (2005) 1093-1102, 10.1038/sj.bjp.0706279.
[31] A.K. Cardozo, V. Buchillier, M. Mathieu, J. Chen, F. Ortis, L. Ladriere, N. Allaman-Pillet, O. Poirot, S. Kellenberger, J.S. Beckmann, D.L. Eizirik, C. Bonny, F. Maurer, Cell-permeable peptides induce dose- and length-dependent cytotoxic effects. Biochim Biophys Acta. 1768 (2007) 2222-2234, 10.1016/j.bbamem.2007.06.003.
[32] A. Hansen, I. Schafer, D. Knappe, P. Seibel, R. Hoffmann, Intracellular toxicity of proline-rich antimicrobial peptides shuttled into mammalian cells by the cell-penetrating peptide penetratin. Antimicrob Agents Chemother. 56 (2012) 5194-5201, 10.1128/aac.00585-12.
[33] Y. Ma, C. Gong, Y. Ma, F. Fan, M. Luo, F. Yang, Y.H. Zhang, Direct cytosolic delivery of cargoes in vivo by a chimera consisting of D- and L-arginine residues. J Control Release. 162 (2012) 286-294, 10.1016/j.jconrel.2012.07.022.
[34] I. Nakase, K. Osaki, G. Tanaka, A. Utani, S. Futaki, Molecular interplays involved in the cellular uptake of octaarginine on cell surfaces and the importance of syndecan-4 cytoplasmic V domain for the activation of protein kinase Calpha. Biochem Biophys Res Commun. 446 (2014) 857-862, 10.1016/j.bbrc.2014.03.018.
[35] S. Ichimizu, H. Watanabe, H. Maeda, K. Hamasaki, K. Ikegami, V.T.G. Chuang, R. Kinoshita, K. Nishida, T. Shimizu, Y. Ishima, T. Ishida, T. Seki, H. Katsuki, S. Futaki, M. Otagiri, T. Maruyama, Cell-penetrating mechanism of intracellular targeting albumin: Contribution of macropinocytosis induction and endosomal escape. J Control Release. 304 (2019) 156-163, 10.1016/j.jconrel.2019.05.015.
[36] A. Erazo-Oliveras, K. Najjar, D. Truong, T.Y. Wang, D.J. Brock, A.R. Prater, J.P. Pellois, The Late Endosome and Its Lipid BMP Act as Gateways for Efficient Cytosolic Access of the Delivery Agent dfTAT and Its Macromolecular Cargos. Cell Chem Biol. 23 (2016) 598-607, 10.1016/j.chembiol.2016.03.016.
[37] J.V. Georgieva, D. Kalicharan, P.O. Couraud, I.A. Romero, B. Weksler, D. Hoekstra, I.S. Zuhorn, Surface characteristics of nanoparticles determine their intracellular fate in and processing by human blood-brain barrier endothelial cells in vitro. Mol Ther. 19 (2011) 318-325, 10.1038/mt.2010.236.
[38] S. Yamaguchi, S. Ito, M. Kurogi-Hirayama, S. Ohtsuki, Identification of cyclic peptides for facilitation of transcellular transport of phages across intestinal epithelium in vitro and in vivo. J Control Release. 262 (2017) 232-238, 10.1016/j.jconrel.2017.07.037.
[39] L. Ledsgaard, M. Kilstrup, A. Karatt-Vellatt, J. McCafferty, A.H. Laustsen, Basics of Antibody Phage Display Technology. Toxins (Basel). 10 (2018), 10.3390/toxins10060236.
[40] J.W. Lee, J. Song, M.P. Hwang, K.H. Lee, Nanoscale bacteriophage biosensors beyond phage display. Int J Nanomedicine. 8 (2013) 3917-3925, 10.2147/ijn.s51894.
[41] B. Oller-Salvia, M. Sanchez-Navarro, S. Ciudad, M. Guiu, P. Arranz-Gibert, C. Garcia, R.R. Gomis, R. Cecchelli, J. Garcia, E. Giralt, M. Teixido, MiniAp-4: A Venom-Inspired Peptidomimetic for Brain Delivery. Angew Chem Int Ed Engl. 55 (2016) 572-575, 10.1002/anie.201508445.
[42] S. Ohtsuki, C. Ikeda, Y. Uchida, Y. Sakamoto, F. Miller, F. Glacial, X. Decleves, J.M. Scherrmann, P.O. Couraud, Y. Kubo, M. Tachikawa, T. Terasaki, Quantitative targeted absolute proteomic analysis of transporters, receptors and junction proteins for validation

of human cerebral microvascular endothelial cell line hCMEC/D3 as a human blood-brain barrier model. Mol Pharm. 10 (2013) 289-296, 10.1021/mp3004308.
[43] B.B. Weksler, E.A. Subileau, N. Perriere, P. Charneau, K. Holloway, M. Leveque, H. Tricoire-Leignel, A. Nicotra, S. Bourdoulous, P. Turowski, D.K. Male, F. Roux, J. Greenwood, I.A. Romero, P.O. Couraud, Blood-brain barrier-specific properties of a human adult brain endothelial cell line. FASEB J. 19 (2005) 1872-1874, 10.1096/fj.04-3458fje.
[44] S. Ogata, S. Ito, T. Masuda, S. Ohtsuki, Changes of Blood-Brain Barrier and Brain Parenchymal Protein Expression Levels of Mice under Different Insulin-Resistance Conditions Induced by High-Fat Diet. Pharm Res. 36 (2019) 141, 10.1007/s11095-019-2674-8.
[45] S. Hanada, K. Fujioka, Y. Inoue, F. Kanaya, Y. Manome, K. Yamamoto, Cell-based in vitro blood-brain barrier model can rapidly evaluate nanoparticles' brain permeability in association with particle size and surface modification. Int J Mol Sci. 15 (2014) 1812-1825, 10.3390/ijms15021812.
[46] A. Lesniak, F. Fenaroli, M.P. Monopoli, C. Aberg, K.A. Dawson, A. Salvati, Effects of the presence or absence of a protein corona on silica nanoparticle uptake and impact on cells. ACS Nano. 6 (2012) 5845-5857, 10.1021/nn300223w.
[47] L.A. Maile, A.W. Aday, W.H. Busby, R. Sanghani, U. Veluvolu, D.R. Clemmons, Modulation of integrin antagonist signaling by ligand binding of the heparin-binding domain of vitronectin to the alphaVbeta3 integrin. J Cell Biochem. 105 (2008) 437-446, 10.1002/jcb.21841.
[48] Y. Xu, J. Xu, W. Shan, M. Liu, Y. Cui, L. Li, C. Liu, Y. Huang, The transport mechanism of integrin alphavbeta3 receptor targeting nanoparticles in Caco-2 cells. Int J Pharm. 500 (2016) 42-53, 10.1016/j.ijpharm.2016.01.028.
[49] P. Kankaanpaa, S. Tiitta, L. Bergman, A.B. Puranen, E. von Haartman, M. Linden, J. Heino, Cellular recognition and macropinocytosis-like internalization of nanoparticles targeted to integrin alpha2beta1. Nanoscale. 7 (2015) 17889-17901, 10.1039/c5nr06218g.
[50] M. Grapp, A. Wrede, M. Schweizer, S. Huwel, H.J. Galla, N. Snaidero, M. Simons, J. Buckers, P.S. Low, H. Urlaub, J. Gartner, R. Steinfeld, Choroid plexus transcytosis and exosome shuttling deliver folate into brain parenchyma. Nat Commun. 4 (2013) 2123, 10.1038/ncomms3123.
[51] X. Dong, Current Strategies for Brain Drug Delivery. Theranostics. 8 (2018) 1481-1493, 10.7150/thno.21254.
[52] L. Kozlovskaya, D. Stepensky, Quantitative analysis of the brain-targeted delivery of drugs and model compounds using nano-delivery systems. J Control Release. 171 (2013) 17-23, 10.1016/j.jconrel.2013.06.028.
[53] C.W. Gan, S.S. Feng, Transferrin-conjugated nanoparticles of poly(lactide)-D-alpha-tocopheryl polyethylene glycol succinate diblock copolymer for targeted drug delivery across the blood-brain barrier. Biomaterials. 31 (2010) 7748-7757, 10.1016/j.biomaterials.2010.06.053.
[54] F. Lu, Z. Pang, J. Zhao, K. Jin, H. Li, Q. Pang, L. Zhang, Z. Pang, Angiopep-2-conjugated poly(ethylene glycol)-co- poly(epsilon-caprolactone) polymersomes for dual-targeting drug delivery to glioma in rats. Int J Nanomedicine. 12 (2017) 2117-2127, 10.2147/ijn.s123422.
[55] K.C. Liu, Y. Yeo, Extracellular stability of nanoparticulate drug carriers. Arch Pharm Res. 37 (2014) 16-23, 10.1007/s12272-013-0286-0.

[56] Y. Sadzuka, I. Sugiyama, T. Tsuruda, T. Sonobe, Characterization and cytotoxicity of mixed polyethyleneglycol modified liposomes containing doxorubicin. Int J Pharm. 312 (2006) 83-89, 10.1016/j.ijpharm.2005.12.043.
[57] M.D. Prados, S.C. Schold, Jr., H.A. Fine, K. Jaeckle, F. Hochberg, L. Mechtler, M.R. Fetell, S. Phuphanich, L. Feun, T.J. Janus, K. Ford, W. Graney, A randomized, double-blind, placebo-controlled, phase 2 study of RMP-7 in combination with carboplatin administered intravenously for the treatment of recurrent malignant glioma. Neuro Oncol. 5 (2003) 96-103, 10.1093/neuonc/5.2.96.
[58] W. Xia, T.A. Springer, Metal ion and ligand binding of integrin alpha5beta1. Proc Natl Acad Sci U S A. 111 (2014) 17863-17868, 10.1073/pnas.1420645111.
[59] M. Nagae, S. Re, E. Mihara, T. Nogi, Y. Sugita, J. Takagi, Crystal structure of alpha5beta1 integrin ectodomain: atomic details of the fibronectin receptor. J Cell Biol. 197 (2012) 131-140, 10.1083/jcb.201111077.
[60] A.S. Sahin, S. Ozkan, Treatment of Obstetric Hemorrhage with Fibrinogen Concentrate. Med Sci Monit. 25 (2019) 1814-1821, 10.12659/msm.914234.
[61] L. Belo, S. Rocha, M.J. Valente, S. Coimbra, C. Catarino, E. Bronze-da-Rocha, P. Rocha-Pereira, M. do Sameiro-Faria, J.G. Oliveira, J. Madureira, J.C. Fernandes, V. Miranda, A. Santos-Silva, Hepcidin and diabetes are independently related with soluble transferrin receptor levels in chronic dialysis patients. Ren Fail. 41 (2019) 662-672, 10.1080/0886022x.2019.1635893.
[62] R.G. Crystal, Adenovirus: the first effective in vivo gene delivery vector. Hum Gene Ther. 25 (2014) 3-11, 10.1089/hum.2013.2527.
[63] R.W. Atchison, B.C. Casto, W.M. Hammon, ADENOVIRUS-ASSOCIATED DEFECTIVE VIRUS PARTICLES. Science. 149 (1965) 754-756, 10.1126/science.149.3685.754.
[64] Y. Tang, T. Han, M. Everts, Z.B. Zhu, G.Y. Gillespie, D.T. Curiel, H. Wu, Directing adenovirus across the blood-brain barrier via melanotransferrin (P97) transcytosis pathway in an in vitro model. Gene Ther. 14 (2007) 523-532, 10.1038/sj.gt.3302888.
[65] K.D. Foust, E. Nurre, C.L. Montgomery, A. Hernandez, C.M. Chan, B.K. Kaspar, Intravascular AAV9 preferentially targets neonatal neurons and adult astrocytes. Nat Biotechnol. 27 (2009) 59-65, 10.1038/nbt.1515.
[66] A.A. Cisek, I. Dabrowska, K.P. Gregorczyk, Z. Wyzewski, Phage Therapy in Bacterial Infections Treatment: One Hundred Years After the Discovery of Bacteriophages. Curr Microbiol. 74 (2017) 277-283, 10.1007/s00284-016-1166-x.
[67] D.M. Lin, B. Koskella, H.C. Lin, Phage therapy: An alternative to antibiotics in the age of multi-drug resistance. World J Gastrointest Pharmacol Ther. 8 (2017) 162-173, 10.4292/wjgpt.v8.i3.162.
[68] M. Shlezinger, L. Khalifa, Y. Houri-Haddad, S. Coppenhagen-Glazer, G. Resch, Y.A. Que, S. Beyth, E. Dorfman, R. Hazan, N. Beyth, Phage Therapy: A New Horizon in the Antibacterial Treatment of Oral Pathogens. Curr Top Med Chem. 17 (2017) 1199-1211, 10.2174/1568026616666160930145649.
[69] X. Wittebole, S. De Roock, S.M. Opal, A historical overview of bacteriophage therapy as an alternative to antibiotics for the treatment of bacterial pathogens. Virulence. 5 (2014) 226-235, 10.4161/viru.25991.

10. Figure captions

Fig. 1 Phage library screening with the hCMEC/D3 cell permeability assay.

(A) Schematic representation of the screening for BBB-permeable cyclic heptapeptides. The phage library was screened three times with the permeability assay with hCMEC/D3 cell monolayer. In the first round, the original library in the medium was added on the apical side

(1.0×10^{11} pfu). The phages, which permeated across the cell monolayer, were collected from the basal side. The permeated phages were used as a prescreened library in the next round. The plaques from selected phages were randomly selected for DNA sequencing. (B) Time course of phage permeation to the basal side during the 1st, 2nd, and 3rd round of screening. The numbers of phages were determined by plaque assay.

Fig. 2 Permeability assay with identified clones from phages that crossed the hCMEC/D3 cell monolayer, as well as the *in vitro* monkey and rat co-culture BBB models.

(A-C) The BBB permeation of two identified phage clones (1.0×10^{11} pfu) was tested with the permeability assay using the *in vitro* human (A, hCMEC/D3 cell), monkey (B, co-culture), and rat BBB models (C, co-culture). The numbers of phages permeated on the basal side were measured by means of qPCR. Closed circle, SLS-phage; closed triangle, NTG-phage; open circle, control phage. Each data point represents the mean ± SEM (n = 3). $^{*}p < 0.05$, $^{**}p < 0.01$, $^{***}p < 0.005$, significantly different from control phages.

Fig. 3 The effect of synthetic cyclic SLS derivative on viability and tight-junction integrity of hCMEC/D3 cells.

(A) hCMEC/D3 cells were incubated with synthetic cyclic SLS derivative for 24 h (circle) or 48 h (square) at indicated concentrations (0–100 μM). Cell viabilities were measured using the cell counting kit-8. Each data point represents the mean ± SEM (n = 6). (B) Effect of the synthetic cyclic SLS derivative on the tight-junction integrity of the hCMEC/D3 cell monolayer. hCMEC/D3 cells were treated with SLS derivative (0–100 μM). After incubation for 48h, TEER values were measured at each timepoint. Each data point represents the mean ± SEM (n=3). Both the TEER and cell viability values did not significantly differ among the various SLS peptide concentrations at the indicated timepoints ($p > 0.05$).

Fig. 4 Characterization of transcellular permeation of SLS-phages across hCMEC/D3 cell monolayer.

(A) Confocal fluorescence microscopic images of SLS-phages internalized into hCMEC/D3 cells. hCMEC/D3 cells were incubated with SLS-phages (1.0×10^{11} pfu) for 10 min at 37 °C. Internalized SLS-phages were visualized by immunostaining (phage, green; nuclei, blue). (B) Effect of low temperature, synthetic cyclic SLS derivative, and EIPA (macropinocytosis inhibitor) on the uptake of SLS-phage by hCMEC/D3 cells. Each data point represents the mean ± SEM (n = 3). $^{****}p < 0.001$, significantly different. (C) Effect of human integrin ligands and holo-transferrin on SLS-phage permeation across hCMEC/D3 cell monolayer (closed circle, SLS-phage; closed square, SLS-phage + Vitronectin; closed triangle, SLS-phage + Fibrinogen; inverted triangle, SLS-phage + RGD; closed diamond, SLS-phage + holo-transferrin; open circle, control phage). The left graph is a magnified graph with a range from 0 to 20 x 10^6 pfu in the right graph. ANOVA did not detect significant differences among the conditions ($p > 0.05$). (D) Effect of monensin on the permeation of SLS-phages and control phages across the hCMEC/D3 cell monolayer (closed circle, SLS-phage; closed diamond, SLS-phage + Monensin; open circle, control phage; open diamond, control phage + Monensin). Each data point represents mean ± SEM (n = 3). $^{**}p < 0.01$, significantly different from SLS-phages. (E) Intracellular titers of SLS-phages and control phages in hCMEC/D3 cell monolayer at 120 min with or without monensin treatment. (F) Hypothesis of the mechanism of SLS-phage permeation across the hCMEC/D3 cell monolayer.

Fig. 5 Distribution of SLS-phages in the mouse brain *in vivo* after intravenous administration.

(A) SLS-phages or control phages (1.0×10^{11} pfu) were administered by i.v. injection, and blood was collected and the brain was excised 60 min post-injection. Plaque assay was performed to determine the phage numbers in the brain and plasma fraction. Each data point represents the mean ± SEM (n = 5–6). $^{**}p < 0.01$, significantly different. (B) Phages in the cerebral cortex and hippocampus section were detected by immunostaining (phage, green; blood vessel, red; nuclei, blue).

Fig. 6 Internalization of FAM-labeled SLS derivative into hCMEC/D3 cells.

(A) Time course of SLS-FAM (10 μM) and FAM (10 μM) uptake by hCMEC/D3 cells (closed circle, SLS-FAM; open circle, FAM). Each data point represents mean ± SEM (n = 3). $^{**}p < 0.01$, $^{***}p < 0.005$, $^{****}p < 0.001$ significantly different from FAM. (B) Confocal fluorescence microscopic images of internalization of SLS-FAM in hCMEC/D3 cells. hCMEC/D3 cells were incubated with SLS-FAM (10 mM) for 5 min at 37 °C. FAM, green; nuclei, blue.

Fig. 7 Permeation of SLS-liposomes across the BBB *in vitro* and *in vivo*.

(A) Time course of 10%-SLS-liposome and control liposome uptake by hCMEC/D3 cells.

Each liposome was labeled with fluorescent DiO, and the proportion of liposome uptake was determined by a fluorescent plate reader. (B-D) SLS-liposome and control liposome permeation across the *in vitro* human (B, hCMEC/D3 cell), monkey (C, co-culture), and rat BBB models (D, co-culture). Closed circle, 10%-SLS-liposome; closed triangle, 1%-SLS-liposome; open circle, control liposome. (E) During the *in vivo* study, the content of each liposome in the brain and plasma was determined at 1 h after i.v. administration into the mice. Each data point represents the mean ± SEM (n = 3). $^{*}p < 0.05$, $^{**}p < 0.01$, $^{***}p < 0.005$, $^{****}p < 0.001$ significantly different from control liposomes.